ADVANCED FUNCTIONAL MATERIALS
www.afm-journal.de

Materials Views
www.MaterialsViews.com

Magnetic Anisotropy of Cr_7Ni Spin Clusters on Surfaces

Valdis Corradini, Alberto Ghirri, Elena Garlatti, Roberto Biagi, Valentina De Renzi, Umberto del Pennino, Valerio Bellini, Stefano Carretta, Paolo Santini, Grigore Timco, Richard E. P. Winpenny, and Marco Affronte*

The problem of the experimental and theoretical determination of magnetic anisotropy in isolated molecular spin clusters is addressed here. To this end, the case of molecular Cr_7Ni rings sublimated in ultrahigh vacuum conditions and assembled in an ordered fashion on Au(111) surface is addressed and investigated using X-ray magnetic dichroism (XMCD) and theoretical calculations. Fixing the experimental conditions at a temperature $T = 8$ K and a magnetic field of 5 T, the angular-dependence of the dichroic signal reveals an easy-axis anisotropy for the Ni magnetization along the direction perpendicular to the ring while the magnetization of the whole Cr_7Ni molecule is preferentially aligned within the ring plane. These features are well reproduced by spin Hamiltonian simulations, which reflect the character of the $S = 3/2$ first excited multiplet, dominating at $T = 8$ K and 5 T. Density functional theory (DFT) calculations show that local spin orbit interactions determine an easy axis anisotropy at the Ni site while the Cr magnetic moment turns out to be more isotropic. This is the first direct observation of the interplay between the single ion and the overall magnetic anisotropy in complex (polynuclear) molecular systems.

1. Introduction

At the end of the 1990s, a new branch of research started with the deposition of molecular nanomagnets (MnM) on surfaces.[1] This, obviously, rose many questions and new challenges: are functionalities intact or tuneable for individual molecules deposited on surface?[2,3] How to control the position, the orientation of their magnetization and the assembling of pre-synthetized molecules on surfaces?[4–6] Is it possible to deposit large molecular complexes in clean conditions? But also: how to use new experimental techniques for measuring the magnetic features of layered assembly of MnM? At the beginning, contradictory results were collected on Mn_{12} deposited on different surfaces.[7–10] It is now clear that some molecules, such as Mn_{12} itself, are not chemically stable when deposited on surfaces while many others, such as Pc_2Tb,[11] Fe_4,[12] Mn_6[13,14] and Cr_7Ni,[3,15,16] are robust enough to sustain a wide range of processes and experiments. Important progress has been recently made on the other fronts: antiferromagnetic molecular complex were successfully deposited in UHV by electro-spray[17] or by sublimation;[18] ii) self assembling of these molecular rings on gold surface have been successfully obtained;[18,19] iii) the orientation of molecules on surfaces was controlled through the anchoring thread in the case of Fe_4[20] or simply by the flat shape of molecular rings.[4,21–23] These achievements open the way for new in-depth studies and for the use of sophisticated experimental techniques. For instance, the X-ray absorption spectra (XAS) provide a unique probe of the electronic and magnetic properties of transition-metal ions with sensitivity down to sub monolayer (sML) coverage. The intensity, lineshape and polarization dependence of dipole-allowed 2p→3d transitions give element-selective information about the spin state, oxidation and ligand field. XMCD has been demonstrated to be a very powerful tool to study magnetic anisotropy on both simple (single magnetic ion) and complex (polynuclear, homometallic) molecules on surfaces.[20,22–26] So far XMCD has been used to measure the total molecular magnetization, i.e., considering the features of the ground state multiplet of the whole molecule.[12,20] Yet, X-ray photons interact with single transition metal ions having their own local magnetic anisotropy projected on the molecular states that, in turns, may have different type of anisotropy one to another. So, the actual alignment of the magnetization of single ion depends on the features of the dominant multiplets at working conditions and it indirectly reflects the characteristics of the whole spin cluster, besides the local environment. This issue is somehow masked in homometallic molecules

Dr. V. Corradini, Dr. A. Ghirri, Dr. V. Bellini
S3 Centre, Institute Nanoscience - CNR,
via G. Campi 213/A, 41125 Modena, Italy
E-mail: valdis.corradini@unimore.it
Dr. E. Garlatti
Dipartimento di Scienze Molecolari Applicate ai Biosistemi
Università di Milano
via Trentacoste 2, 20134 Milano, Italy
Dr. R. Biagi, Dr. V. De Renzi, Prof. U. del Pennino, Prof. M. Affronte
Dipartimento di Fisica
Università di Modena e Reggio Emilia and S3 Centre
Institute Nanoscience - CNR via G. Campi 213/A, 41125 Modena, Italy
Prof. S. Carretta, Prof. P. Santini
Dipartimento di Fisica
Università di Parma
v.le delle Scienze, 43100 Parma, Italy
Dr. G. Timco, Prof. R. E. P. Winpenny
School of Chemistry and Photon Science Institute
University of Manchester
Oxford Road, Manchester, M13 9PL, UK

DOI: 10.1002/adfm.201200478

but it can be properly addressed in heterometallic ones, such as Cr_7Ni rings[5] and Fe_3Cr.[2,27] Interestingly, the chemical specificity of XMCD allows to elucidate this interplay between the magnetization of the single ion and that of the entire molecule. While the importance of magnetic anisotropy for large spin single molecule magnets is well recognized, it is worth noting that the control and the understanding of magnetic anisotropy is also relevant for the spin manipulation in molecular qubits like the antiferromagnetic Cr_7Ni.

In this work we present an in-depth investigation on magnetization alignment in Cr_7Ni molecular rings deposited on surfaces. We take advantage of several special conditions. Firstly, the extra magnetic ion (Ni^{2+}) unbalances the Cr ring magnetization and acts as local probe inside the ring, as demonstrated in our previous works.[28] Secondly, we recently succeeded in assembling Cr_7Ni rings in ordered fashion on Au(111) surface by UHV sublimation.[18] Namely, no changes are observed on the chemical features and only minor variations are observed on magnetism of isolated Cr_7Ni rings that lay all flat and well packed (hexagonal arrangement) on gold surface (**Figure 1**).[18] Moreover, for this experimental investigation we have made use of different types of molecule-surface interaction, namely two different functionalizations of the rings deposited on Au(111) and HOPG substrates. Since the ground state of Cr_7Ni is an isotropic doublet, we worked at finite temperature and magnetic field in such a way that the first excited S = 3/2 multiplet, with in-plane anisotropy, is the dominant one. Spin Hamiltonian simulations are then used to clarify the alignment of the Ni magnetization and the interplay between the local and the molecular magnetic anisotropy, while DFT calculations explain the origin of the local electronic and magnetic features.

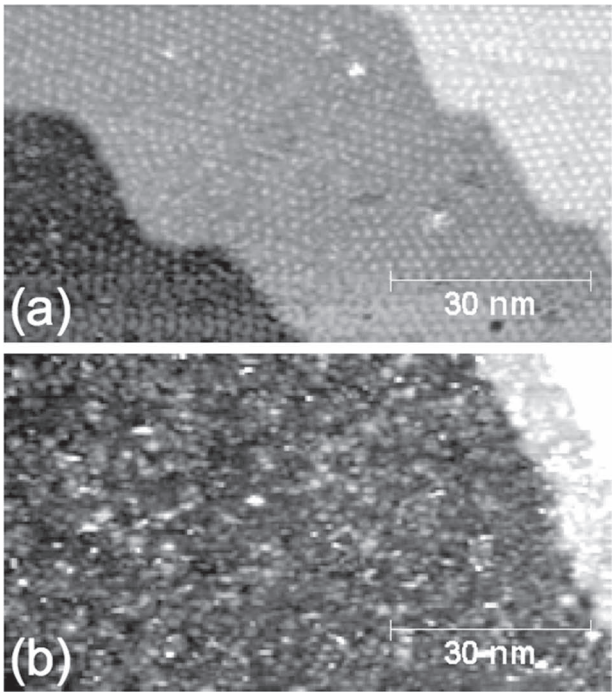

Figure 1. STM image of one complete self-assembled monolayer of Cr_7Ni-bu (upper panel) and Cr_7Ni-thiobu (lower panel) deposited by sublimation on Au(111) surface. Tunneling conditions: 2 V and 20 pA. Scan area 90×50 nm^2.

2. Experimental Results

Synthesis and crystallographic structure of:

Cr_7Ni-bu $\{[(CH_3)_2CHCH_2]_2NH_2\}$
$\{Cr_7NiF_8[O_2CC(CH_3)_3]_{16}\}$ and

$Cr_7Ni-thiobu$ $\{HSCH_2CH_2NH_2CH_2CH_2CH_2CH_3\}$
$\{Cr_7NiF_8[O_2CC(CH_3)_3]_{16}\}$

are described in detail in ref. [18]. As shown in the STM image of Figure 1, the Cr_7Ni-bu derivative on Au(111), weakly bound to the surface, forms a highly ordered 2D hexagonal layer. On the other hand, in the case Cr_7Ni-thiobu covalent bonding between molecules and the gold adatoms leads to a strong molecular grafting and to the formation of a disordered monolayer.[18] In both cases, STM imaging and DFT calculations indicate that molecular Cr_7Ni rings lay flat on the gold surface, as this configuration maximizes the contact surface between the molecules and the substrate.[18] Conversely, in the case of Cr_7Ni-bu deposited on HOPG, the weak molecule-surface interaction does not allow to obtain stable STM images of the molecular rings.

We define the *z*-axis along the direction of the incident X-ray beam, which is parallel to the applied magnetic field vector (**H**) in our experimental set up, and *z′* the normal to the surface which, in case the of molecules laying flat on the surface, coincides with the axis perpendicular to the ring plane. The thick films (TF) were obtained fixing microcrystalline powders on carbon-tape.

2.1 XAS and XMCD Spectra

In **Figure 2** the Cr and Ni $L_{2,3}$ XAS and XMCD spectra for the two monolayers (MLs) (i.e., Cr_7Ni-bu and Cr_7Ni-thiobu) on Au(111) and the Cr_7Ni-bu ML on the HOPG surface are compared with those of the corresponding microcrystalline thick film (TF). Remarkably, both the XAS and XMCD spectral line-shapes for MLs perfectly resemble those of the TFs, demonstrating that deposition by sublimation does not affect the valence electronic structure of the Cr and Ni ions, namely oxidation state, local environment and crystal-field intensity at the Cr and Ni sites. More specifically, for all samples the Cr absorption spectra present eight features characteristic of Cr^{3+} in a nearly O_h environment, whereas Ni spectra present two peaks at the L_3 edge and a partially resolved doublet structure at the L_2 edge, characteristic of a high-spin Ni^{2+} ion in nearly O_h symmetry.[29]

In these molecular rings, when an external magnetic field **H** is applied, there is a competition between the antiferromagnetic coupling between nearest-neighboring ions and the Zeeman interaction, tending to align the magnetic moments along the field direction. The XMCD spectra of Figure 2b provide information on this competition. The negative dichroic signal at the Cr L_3 edge and the positive one at the L_2 edge [$L_3(-)$, $L_2(+)$] implies that the total magnetic moment of the Cr ions is parallel to **H**. Conversely, the opposite behavior of Ni [$L_3(+)$, $L_2(-)$],

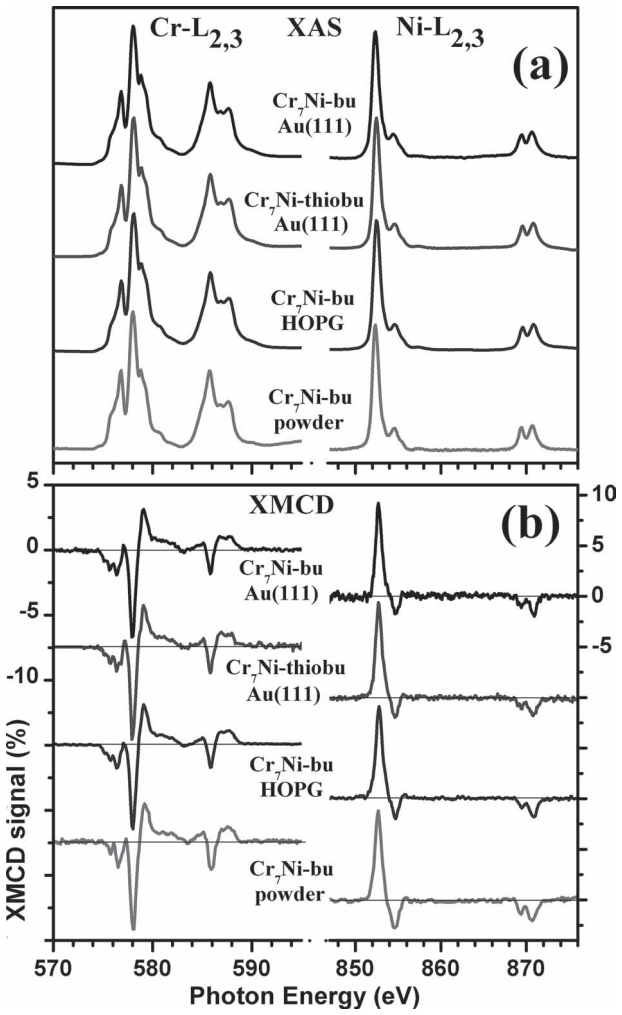

Figure 2. Cr (left) and Ni (right) $L_{2,3}$ XAS (a) and XMCD (b) spectra, measured at 8 K and 5 T on 1ML of Cr_7Ni-bu and Cr_7Ni-thiobu on Au(111), 1ML Cr_7Ni-bu on HOPG deposited by sublimation. The spectrum of Cr_7Ni-bu powders is also shown for comparison.

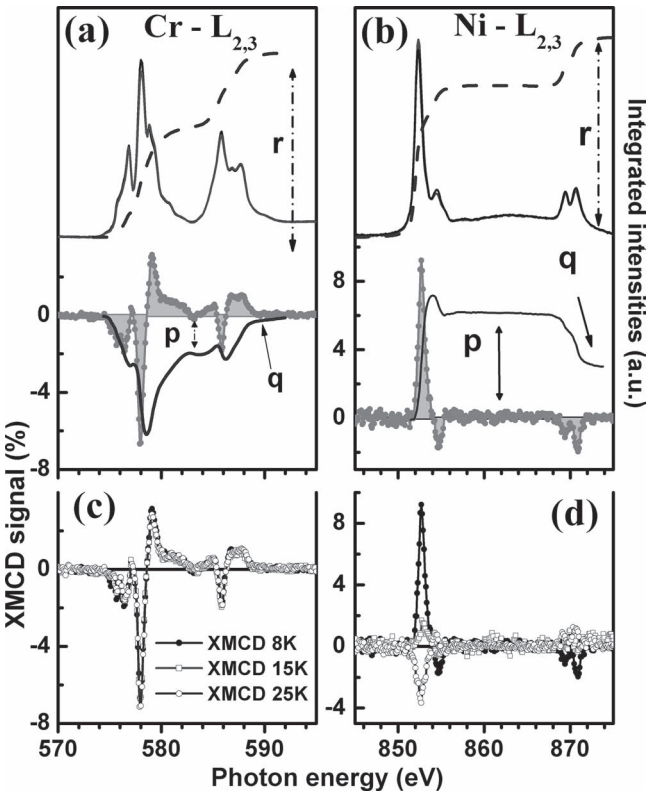

Figure 3. Upper panels: Cr (a) and Ni (b) $L_{2,3}$ XAS spectra taken with $\sigma^{\uparrow\uparrow}$ and $\sigma^{\uparrow\downarrow}$ circularly polarized light and the XAS integral (dashed line) at 5 T and 8 K for 1ML Cr_7Ni-bu on Au(111). XMCD spectra ($\sigma^{\uparrow\downarrow} - \sigma^{\uparrow\uparrow}$) and their integrals (continuous lines). The parameters *p*, *q*, and *r* are the values used for the sum rules analysis. Lower panels: Cr (c) and Ni (d) XMCD spectra measured at 8 K, 15 K, and 25 K in 5 T magnetic field.

for either powders and MLs, implies that at 8K the magnetic moment of the Ni ion is antiparallel to **H**.

2.2 Temperature and Magnetic Field Dependence of XMCD Spectra

Figure 3a,b show the Cr-$L_{2,3}$ and Ni-$L_{2,3}$ absorption spectra taken using both photon helicities (upper panel), the relative dichroic signal and its integral (lower panel) measured for 1ML Cr_7Ni-bu on Au(111) at 8 K and 5 T. In Figure 3c,d, the XMCD spectra of Cr and Ni are displayed at three temperatures: 8 K, 15 K, and 25 K. Similar measurements were performed also for the other ML samples and for the TFs. We observe that, while the total Cr magnetic moment is always parallel to **H**, for Ni the magnetic moment is antiparallel to **H** at 8 and 15 K but it becomes parallel to **H** at 25 K (see Figure 3d). These results can be quantitatively analysed exploiting XMCD sum rules for each type of magnetic ion.[29] The mean value of the spin (m_S) and orbital (m_O) moments (along the z direction) are given by:[30]

$$\frac{m_o}{\mu B} = -\frac{4q \cdot N_{eff}}{3r}$$

$$\frac{ms}{\mu B} = -\frac{(6p-4q)\cdot N_{eff}}{r}.\ Sc + \frac{7\langle Tz\rangle}{\mu B}$$

where $r = I_{L3} + I_{L2}$ is the integral of the whole absorption spectrum, A and B are the intensities of the dichroic signal at the L_3 and L_2 edges, respectively, and $p = A$ and $q = A+B$ (see Figure 3a,b). We have already discussed the validity of the sum rules for Cr_8,[29] Cr_7Ni,[31] Cr_xInNi[32] and Cr_2Cu[33] where we derived a spin correction factor (S_C) of 1.75 for Cr to account for the partial L_2 and L**3** mixing. For what concerns the 3d-hole numbers, we considered the nominal values $N_{eff} = 7$ for Cr^{3+} and $N_{eff} = 2$ for Ni^{2+}.

For the general case of 3d metals, the dipolar term T_Z is expected to be different from zero, however, in the case of Cr^{3+} ions in O_h symmetry, it results negligible[34] allowing the application of the isotropic sum rules for Cr. On the contrary, for $3d^8$ metal, e.g., Ni^{2+} ions, T_Z is not negligible even in O_h symmetry. On the basis of theoretical calculations,[34] in the spin moment sum rule we consider a negative 7 T_Z term of –0.06 μ_B, which is about 1/30 of the m_S value: $7T_Z/m_S = -0.03$.

The q value of the dichroic signal at the Cr-$L_{2,3}$ edges is related to the orbital moment m_O of the Cr^{3+} ions. Its vanishing value

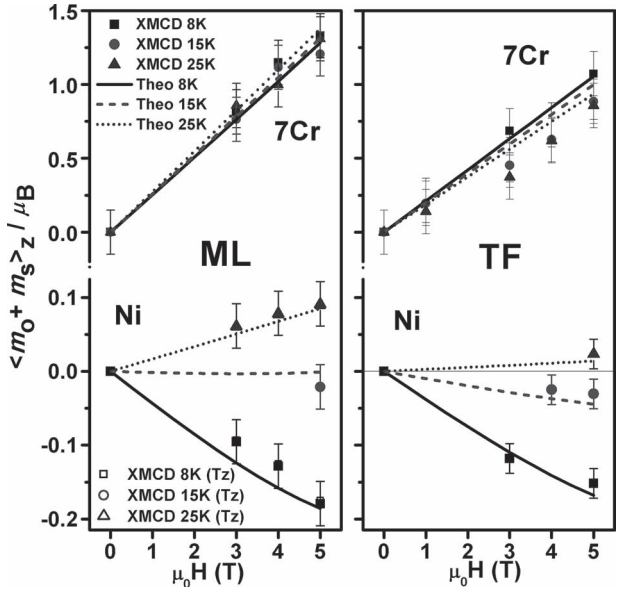

Figure 4. Total magnetic moments derived by using the sum rules for 7 Cr and 1 Ni with (open symbols) and without (filled symbols) considering Tz, plotted as a function of the applied magnetic field at 8 K, 15 K, and 25 K and compared with the results of spin-Hamiltonian calculations (continuous lines). 1ML Cr_7Ni-bu on Au(111) (left panel) and Cr_7Ni-bu powders (right panel) are reported.

indicates a complete quenching of m_O due to crystal field effects. On the contrary m_O of Ni^{2+} ions is only partially quenched. This occurs for all the MLs and powders investigated. For all systems the m_O value derived by the sum rules is about 10 ÷ 15% of m_S, for all the spanned temperatures and magnetic field **H**. Thus Cr ions have a nearly spin-only gyromagnetic factor (g_{Cr} = 2.0), whereas for Ni g_{Ni} = 2.25 ± 0.05. These values are very close to the ones derived for the pristine (bulk) Cr_7Ni-piv derivative and, incidentally, confirm that neither thermal sublimation nor the interaction with the Au surface affects the degree of quenching of the orbital momentum.

Figure 4 displays the behavior of the Cr and Ni magnetic moments, for 1ML of Cr_7Ni-bu on Au(111) and the corresponding thick films (TF), as a function of an external magnetic field **H** at different temperatures. It is worth noting that the Cr total magnetic moment is larger in the ML than in the TF and it is parallel to **H**, at all the temperatures considered. A different behavior is observed for Ni in the ML: negative values, i.e., moment antiparallel to **H**, are observed at 8 and 15 K, while as temperature increases, an inversion in the sign of the Ni dichroism at 25 K occurs. This behavior reproduces that observed in the TF, and shows that the increasing temperature induces different alignment of the Ni magnetization to the external field. A very similar behavior has been observed also for 1ML of Cr_7Ni-thiobu on Au(111) and of Cr_7Ni-bu on HOPG (see SI).

3. Spin Hamiltonian and Numerical Simulations

We can describe the magnetic properties of each Cr_7Ni ring by the Spin Hamiltonian (s_{Cr} = 3/2 and s_{Ni} = 1):

$$H = \sum_i J_{i,i+1}\mathbf{s}_i \cdot \mathbf{s}_{i+1} + \sum_i d_i \left(s_{z',i}^2 - \frac{1}{3} s_i (s_i + 1) \right) + \mu_B \sum_i g_i \mu_0 \mathbf{H} \cdot \mathbf{s}_i \quad (1)$$

where the first term represents the dominant isotropic nearest-neighbor anti-ferromagnetic exchange interaction, the second term accounts for axial anisotropy (being *z'*- the axis perpendicular to the ring plane) and the last one is the Zeeman coupling to an external field $\mu_0\mathbf{H}$. Since XMCD results show that the degree of orbital momentum quenching is the same as in the original Cr_7Ni-piv molecule, the gyromagnetic factors g_i have been fixed to 1.98 (Cr^{3+}) and 2.2 (Ni^{2+}).[29,35]

As shown in Figure 4, the experimental results on TF samples (right panel) are well reproduced by Equation 1, using $J_{Cr\text{-}Cr}$ = 1.46 meV and $J_{Cr\text{-}Ni}$ = 1.69 meV, values obtained from bulk measurements.[28,35–37] The temperature dependence of magnetic moments measured on the ML is slightly different: reasonably the direct interaction of molecules with the gold surface induces a slight change in the *J*'s constants. So, the experimental data for 1ML Cr_7Ni-bu on Au(111) in the left panels of Figure 4 are well fitted by using exchange constants $J_{Cr\text{-}Cr}$ = 1.14 meV and $J_{Cr\text{-}Ni}$ = 1.32 meV in Equation 1, which present a small -but sizeable reduction (22%) for both J's constant with respect to the (TF) bulk. The uncertainty on the TF and ML fitting parameters is of the order of 10% as variations within this range keep the fit acceptable. It is important to note that both TF and ML data are well reproduced by assuming the same d_{Cr} = –0.03 meV and d_{Ni} = –0.35 meV in Equation 1, as derived from bulk measurements,[38] i.e., changes in *d'* values make the fit systematically worst.

It is worth to stress that the structure of the low-energy levels of the grafted rings, shown in **Figure 5**, is not modified by the reduction of the exchange coupling constants and it remains practically the same as in the original Cr_7Ni rings in bulk crystals. This small reduction of *J* values only leads to a small compression of the spectrum (e.g., the ground-doublet to first excited-quartet gap $\Delta_{1/2-3/2}$ becomes about 11 K instead of 14 K).

4. Angular Dependence of X-Ray Dichroism

In our experiments the magnetic field **H** direction is always parallel to the beam, whereas the angle θ between the surface normal and **H** can be varied between 0° and 75° (**Figure 6**b). The dependence of the XAS and XMCD spectral shape on θ has been studied for all MLs and for the TFs, and it is shown in Figure 6a for Cr and in Figure 6c–e for Ni. The information on the magnetic moment anisotropy of Cr (Figure 6a) is averaged over seven ions and it results practically zero. Conversely, the Ni XMCD signal shows a clear dependence on θ: in the case of 1ML Cr_7Ni-bu and 1ML Cr_7Ni-thiobu (Figure 6c,d) on Au(111), a strong angular dependence is observed with 40% reduction passing from θ = 0° to θ = 75°, while for Cr_7Ni-bu on HOPG a modest angular dependence (12% reduction) is observed. No dependence on θ is observed in the case of randomly oriented polycrystalline thick film. These findings

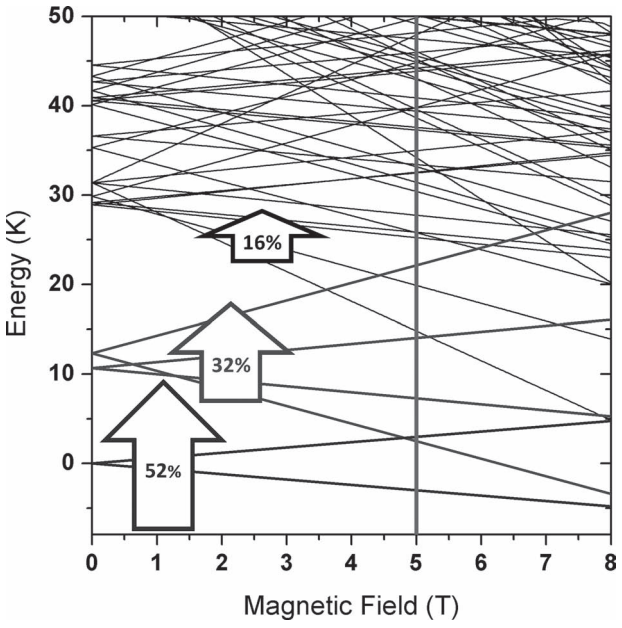

Figure 5. Zeeman plot (magnetic field dependence) of the low-lying energy levels calculated for 1ML Cr_7Ni-bu on Au(111). Parameters used in calculations are $J_{Cr\text{-}Cr} = 1.14$ meV and $J_{Cr\text{-}Ni} = 1.32$ meV. Arrows indicate the occupancy calculated at 5 T and 8 K for different multiplet.

confirm that, in the case of deposition on gold, the molecular rings lay flat on the surface, with their z'-axis perpendicular to the latter.[18] In the case of graphite, the molecular rings tend to be less oriented, representing an intermediate situation between gold and bulky powders, where rings are randomly oriented.

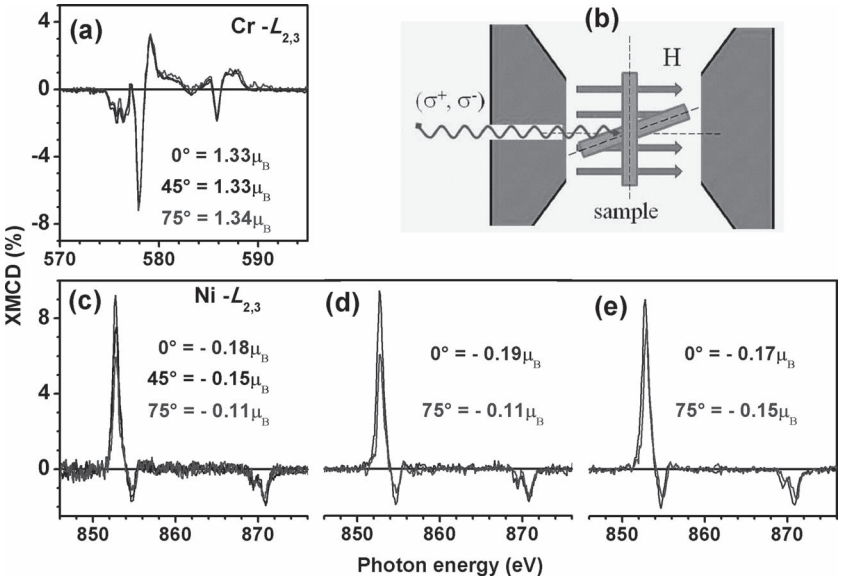

Figure 6. XMCD spectra at the Cr (a) and Ni (c) $L_{2,3}$ edges measured on 1ML Cr_7Ni-bu on Au(111) for different angles θ of the applied magnetic field; (d) 1ML Cr_7Ni-thiobu on Au(111) and (e) 1ML Cr_7Ni-bu on HOPG. The values indicated are the total magnetic moments derived by sum rules (the error bar is $\pm 0.05\ \mu_B$ ($\pm 0.02\ \mu_B$) for Cr (Ni) edge). b) Experimental geometry with the two limit situations: $\theta = 0$ (H and beam normal to the surface) and $\theta = 75°$.

Again, we can make use of the XMCD sum rules to derive the m_S and m_O moments for each type of magnetic ion as a function of θ. The results are reported in **Table 1** and **Figure 7**. As expected the m_S of the 7Cr ions does not change with θ whereas the Ni magnetic moment decreases as θ increases indicating the magnetic moment of Ni preferentially aligns along the z'-axis. Summing up the 7Cr and the Ni magnetic moments, the total magnetization of the Cr_7N ring results lower at $\theta = 0°$ than at $\theta = 75°$(see Table 1), indicating an easy plane for the ring magnetization in this experimental conditions, i.e., T = 8K and $\mu_0\mathbf{H}$ = 5T.

The angular dependence of the different magnetic moments for the Ni ion, each Cr site, the 7Cr complex and the whole Cr_7Ni ring, have been theoretically evaluated by Equation 1 at T = 8 K as a function of the applied magnetic field (**Figure 8**). These calculations show that single ion magnetic moments have alternating signs with a negative sign for Ni (meaning that the Ni moment is anti-parallel to the field direction). The absolute value of the magnetic moment for each Cr ion depends on its distance from the Ni one (see inset in Figure 8). For instance, the two Cr ions right next to it have the largest moments. In summary, Figure 7a–c shows a very good agreement between calculations and experimentally derived θ dependence of the different moments.

Exploiting the parameters obtained by fitting the sum rule results, it is possible to understand the origin of the easy plane anisotropy of the Cr_7Ni ring. The effective magnetic anisotropy of each total-spin multiplet in molecular nanomagnets can be evaluated by projecting single-ion crystal field terms on the chosen multiplet, thus evaluating their effective zero-field splitting parameter D:

$$D = d_{Cr}\sum_{i=1}^{7}\Gamma_i + d_{Ni}\Gamma_{Ni} \quad (2)$$

Γ_i(k,S) are projection coefficients that are constant inside each S multiplet.[39,40] S-mixing effects in Cr_7Ni are small and can therefore be neglected in the evaluation of the effective anisotropy. In the experimental conditions ($\mu_0\mathbf{H}$ = 5 T and T = 8 K) the two mainly populated multiplets are the ground S = 1/2 doublet and the first-excited S = 3/2 quartet (see Figure 5). Our calculations indicate that for the S = 3/2 multiplet all Γ_i coefficients are negative while they vanish in the ground doublet for the time-reversal symmetry. Hence, the resulting easy plane anisotropy of the whole Cr_7Ni ring at T = 8K and H = 5T is determined by the effective magnetic anisotropy of S = 3/2 multiplet for which D > 0 (all the d parameters and projection coefficients in Equation 2. are negative). Indeed, in zero field, anisotropies cause a splitting between the | 3/2, ±1/2 > and the | 3/2, ±3/2 > states with a gap of 0.15 meV (or 1.7 K) and the | 3/2, ±1/2> state is the lower in energy (see Figure 5).

5. Density Functional Calculations

In order to get deeper insight on the origin of magnetic anisotropy, we have carried out a density-functional characterization of the

Table 1. Ni and 7Cr spin, orbital and total magnetic moments, experimentally derived by the sum rules for 1ML Cr_7Ni-bu on Au(111) as a function of θ, the angle between the direction of the beam (which coincides with H) and the normal to surface at 8 K and magnetic field 5 T.

Sum rules		Angle (θ)			
		0°	45°	75°	summary
	m_S	–0.16	–0.135	–0.1	
	m_o	–0.02	–0.015	–0.01	
Ni	m_t	–0.18	–0.15	–0.11	easy axis
7Cr	m_t	1.33	1.33	1.34	
Cr_7Ni	m_t	1.15	1.18	1.23	easy plane

isolated Cr_7Ni-bu molecule, and extracted expectation values of spin and orbital moments and single-ion anisotropy energy barriers (E_B) at Cr and Ni ions. The presence of substrate is neglected for simplicity and in light of the experimental findings discussed before. The calculations have been carried out using the Wien2K code.[41] Exploiting the space subdivision in muffin-tin (MT) spheres/interstitial region intrinsic in the augmented-plane-wave basis set employed, it is possible to switch on spin-orbit interaction separately either on one Cr ion or on the Ni ion and extract form total energy differences their single-ion anisotropies. Since experimentally the molecules are rotated in the surface plane without any preferential azimuthal angle and considering that variation of orbital moment and total energies appear as a function of the azimuthal angle in the calculation, in the following in-plane values have been averaged over two orthogonal in-plane magnetization axis directions. As discussed previously, octahedrally coordinated Cr^{3+} has a very low orbital moment that we find to amount to only 0.02–0.03 μ_B, which is approximately 1/100 of the spin expectation values (2.9μ_B within the MT sphere, while it is nominally 3.00 μ_B). This suits nicely with the chosen gyromagnetic value for Cr (g = 1.98); no sensible variations is observed varying the angle between the magnetization and the molecule axes, the E_B is less than 0.1 meV and point to an easy magnetization along the z'-axis perpendicular to the molecular plane.[42] In the case of Ni^{2+}, the spin moment is, as expected, isotropic (1.75 μ_B, while it is nominally 2.00 μ_B), yet the orbital moment is around 0.20μ_B if the magnetization axis is perpendicular to the molecule plane, while it averages to 0.14μ_B if the magnetization axis is chosen to be in-plane, the anisotropy E_B is around 0.7 meV. These results fully support the choice of the *d* values used in Equation 1 and they can be qualitatively understood also in terms of the Bruno model,[43] which states that the expectation value of the orbital moment has its maximum along the magnetization easy axis. Moreover, the comparison with the larger variation (for smaller angle differences, i.e. experimental 0°–75° *cf.* theoretical 0°–90°) of the measured orbital moment presented in Table 1, suggests that most likely also orbital moments, as much as spin moments, have not reached saturation at the experimental applied field of 5T.

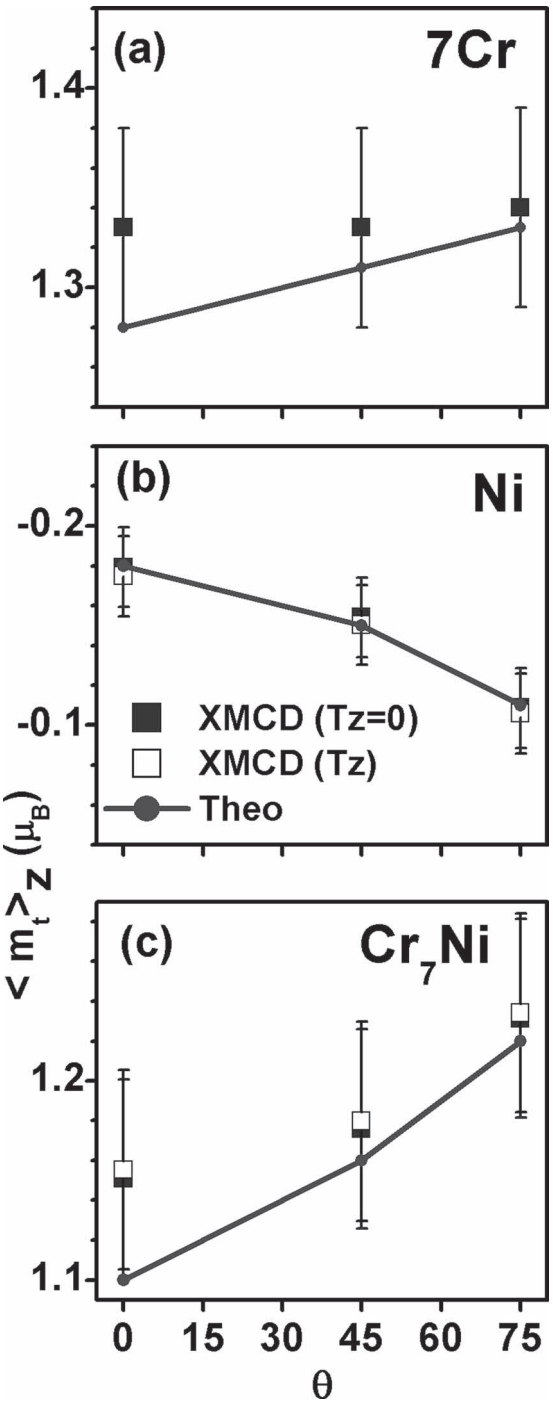

Figure 7. Total magnetic moment derived by the sum rules for 7Cr (a), Ni (b), and the whole Cr_7Ni (c) with (open symbols) and without (filled symbols) considering Tz, compared with the results of the spin-Hamiltonian calculations (continuous lines).

6. Conclusions

Deep analysis of the angular dependence of XMCD spectra of ordered MLs of Cr_7Ni molecular rings allowed us to elucidate the relationship between the magnetization of the single ions and that of the entire molecule. This study is in line with the recent use of XMCD technique on heterometallic molecular systems[2,27] but here we can exploit the advantage that the deposition by sublimation induces an ordered self-assembling with an alignment of the Cr_7Ni rings on the surface. Experimen-

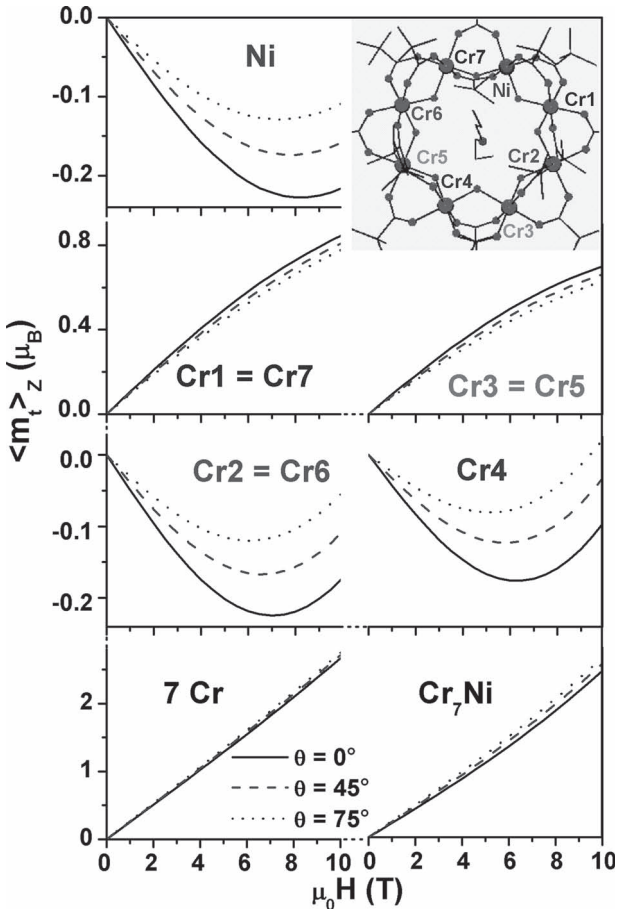

Figure 8. Angular dependence of the total magnetization calculated by spin-Hamiltonian at 8 K for the Ni, for each Cr site, for the 7Cr and for the whole Cr_7Ni ring. Inset: the ring structure showing the different Cr positions with respective numbers.

tally, at 8 K and 5 T, the magnetic moment of Ni tends to align along the z'-axis perpendicular to the ring plane, whilst the total magnetic moment of the molecule prefers to align within that plane. This apparent discrepancy is reconciled as follows: both Ni and single-Cr magnetic moments have easy-axis anisotropy [weak for Cr: $d_{Cr} = -0.03$ meV and stronger for Ni: $d_{Ni} = -0.35$ meV in Equation (1)], as corroborated by DFT calculations. Projecting these anisotropies on the S = 3/2 multiplet, which dominates in our experimental conditions, we obtain an easy-plane anisotropy for the magnetization of the whole molecule, in perfect agreement of our experimental findings. These results evidence that X-ray dichroism probe magnetic features of single ion whilst the magnetic anisotropy of molecular cluster results from projection of these anisotropies on the dominant multiplet at fixed experimental conditions (temperature and magnetic field). Whilst this finding is probably not particularly surprising, our description of this interplay involves the use of the XMCD sum rules, diagonalization of spin Hamiltonian, projection of local anisotropies on molecular multiplets and ab initio DFT calculations. So, remarkably the overall theoretical description turns out to be self-consistent and perfectly fits the experimental results that, in turns, provide, to our knowledge, the first direct observation of such interplay. More specifically this work elucidates the origin of magnetic anisotropy in antiferromagnetic Cr_7Ni rings, evidencing a weak anisotropy of the magnetic moments at the Cr sites, that is a further element for the easy manipulation of the molecular spin as required for the use of these molecular spin clusters for quantum information processing.[44]

7. Experimental Section

Two kinds of Cr_7Ni derivatives with different functionalizations (Cr_7Ni-bu and Cr_7Ni-thiobu) were evaporated on both Au(111) single crystal and Highly Oriented Graphite samples. The surface of Au(111) single crystals was prepared by repeated sputtering (Ar^+) and annealing (430 °C) cycles until the herringbone (22×√3) reconstruction was observed (by STM or LEED). The HOPG substrates, purchased from NT-MDT (grade ZYA), were freshly cleaved before use. Cr_7Ni-bu and Cr_7Ni-thiobu powders were evaporated, after purification, by means of a resistively heated borosilicate glass vial, mounted on a differentially pumped stage, normally separated from the experimental UHV chamber by a gate valve which was opened only during deposition. The sublimation temperature was controlled by a thermocouple embedded into the vial. In this setup the deposition rate is about 1 ML in 60 min for the Cr_7Ni-bu (Cr_7Ni-thiobu) sublimated at 200 °C (185 °C). STM images were taken on the Au(111) samples at room temperature in UHV by means of an Omicron VT-SPM microscope working in constant-current mode.

XMCD experiments were carried out at the ID8 beamline of the European Synchrotron Radiation Facility in Grenoble, France. The lowest sample temperature was about 8 K, and the base pressure of the experimental chamber was 1.0×10^{-9} mbar during sublimation and 1.0×10^{-10} mbar during measurements. The photon source was an Apple II undulator that delivers a high flux of polarized light. We paid much attention to avoid any sample degradation induced by radiation exposure, working with very low flux (below 10^{12} photons/s) and strictly monitoring XAS spectra throughout all the experiments to detect any trace of sample damaging. XMCD measurements at the Cr and Ni $L_{2,3}$ edges were performed in total electron yield mode using circularly polarized light with about 100% polarization rate and with an external magnetic field $\mu_0 H$ up to 5 T applied perpendicularly to the sample surface and parallel to the incident photon beam. The dichroic spectrum is the difference between the XAS spectra taken with the helicity of the incident photon antiparallel ($\sigma^{\uparrow\downarrow}$) and parallel ($\sigma^{\uparrow\uparrow}$) to the sample magnetization. In order to minimize the effects of field inhomogeneity, we carried out measurements by switching both the helicity and the applied field. The angular dependence of the magnetization was probed by varying the the sample orientation with respect to X-ray beam incidence direction.

Diagonalization of Spin Hamiltonian: The theoretical evaluation of the temperature and magnetic field dependence of Cr and Ni magnetic moments required the diagonalization of Equation 1. If the magnetic field $\mu_0\mathbf{H}$ was along the z'-axis ($\theta = 0$), the total spin operator $S_{z'}$ commuted with the hamiltonian H. Thus Equation 1 could be exactly diagonalized within each block with fixed M, where M is the eigenvalue of $S_{z'}$. However when the magnetic field $\mu_0\mathbf{H}$ was along a different direction ($\theta \neq 0$), $[\Sigma_i g_i \mathbf{H}\cdot\mathbf{s}_i, S_z'] \neq 0$ diagonalization of Equation 1 was obtained by a solution scheme based on an irreducible tensor operators (ITOs) formalism.[45] Using these two diagonalization methods it is possible to obtain both eigenvalues and eigenstates of Equation 1 at the different θs from which one can estimate the local magnetization at single Cr and Ni sites. It was verified that for $\theta = 0°$ both methods yield the same results.

Supporting Information

Supporting Information is available from the Wiley Online Library or from the author.

Acknowledgements

The authors acknowledge the European Synchrotron Radiation Facility for provision of beam time allocation and They would like to thank Julio Criginsky Cezar for assistance during experiment HE-3521 at ID8 beamline.

Received: February 16, 2012
Revised: April 4, 2012
Published online: May 21, 2012

[1] N. Domingo, E. Bellido, D. Ruiz-Molina, *Chem. Soc. Rev.* **2011**, *41*, 258.
[2] A. Cornia, M. Mannini, P. Sainctavit, R. Sessoli, *Chem. Soc. Rev.* **2011**, *40*, 3076.
[3] V. Corradini, F. Moro, R. Biagi, V. De Renzi, U. del Pennino, S. Carretta, P. Santini, V. A. Milway, G. Timco, R. E. P. Winpenny, M. Affronte. *Phys. Rev. B* **2009**, *79*, 144419.
[4] M. Gonidec, R. Biagi, V. Corradini, F. Moro, V. De Renzi, U. del Pennino, D. Summa, L. Muccioli, C. Zannoni, D. B. Amabilino,, J. Veciana, *J. Am. Chem. Soc.* **2011**, *133*, 6603.
[5] M. Cavallini, J. Gomez-Segura, D. Ruiz-Molina, M. Massi, C. Albonetti, C. Rovira, J. Veciana, F. Biscarini, *Angew. Chem. Int. Ed.* **2005**, *44*, 888.
[6] V. Corradini, U. del Pennino, R. Biagi, V. De Renzi, A. Gambardella, G. Gazzadi, A. Candini, L. Zobbi, A. Cornia, *Surf. Sci.* **2007**, *601*, 2618.
[7] Z. Salman, K. H. Chow, R. I. Miller, A. Morello, T. J. Parolin, M. D. Hossain, T. A. Keeler, C. D. P. Levy, W. A. MacFarlane, G. D. Morris, H. Saadaoui, D. Wang, R. Sessoli, G. G. Condorelli, R. F. Kiefl, *Nano Lett.* **2007**, *7*, 1551.
[8] L. Bogani, L. Cavigli, M. Gurioli, R. L. Novak, M. Mannini, A. Caneschi, F. Pineider, R. Sessoli, M. Clemente-Leon, E. Coronado, A. Cornia, D. Gatteschi, *Adv. Mater.* **2007**, *19*, 3906.
[9] S. Voss, M. Fonin, U. Rudiger, M. Burgert, U. Groth, Y. S. Dedkov, *Phys. Rev. B* **2007**, *75*, 45102.
[10] E. Coronado, A. Forment Aliaga, F. M. Romero, V. Corradini, R. Biagi, V. De Renzi, A. Gambardella, U. del Pennino, *Inorg. Chem.* **2005**, *44*, 7693.
[11] R. Biagi, J. Fernandez-Rodriguez, M. Gonidec, A. Mirone, V. Corradini, F. Moro, V. De Renzi, U. del Pennino, J. C. Cezar, D. B. Amabilino,, J. Veciana, *Phys. Rev. B* **2010**, *82*, 224406.
[12] M. Mannini, F. Pineider, Ph. Sainctavit, C. Danieli, E. Otero, C. Sciancalepore, A. M. Talarico, M.-A. Arrio, A. Cornia, D. Gatteschi, R. Sessoli, *Nat. Mater.* **2009**, *8*, 194.
[13] F. Moro, V. Corradini, M. Evangelisti, R. Biagi, V. De Renzi, U. del Pennino, J. C. Cezar, R. Inglis, C. J. Milios, E. K. Brechin, *Nanoscale* **2010**, *2*, 2698.
[14] F. Moro, V. Corradini, M. Evangelisti, V. De Renzi, R. Biagi, U. del Pennino, C. J. Milios, L. F. Jones, E. K. Brechin, *J. Phys. Chem. B* **2008**, *112*, 9729.
[15] V. Corradini, R. Biagi, U. del Pennino, V. De Renzi, A. Gambardella, M. Affronte, C. A. Muryn, G. A. Timco, R. E. P. Winpenny, *Inorg. Chem.* **2007**, *46*, 4937.
[16] A. Ghirri, V. Corradini, C. Cervetti, A. Candini, U. del Pennino, G. Timco, R. J. Pritchard, C. A. Muryn, R. E. P. Winpenny, M. Affronte, *Adv. Funct. Mater.* **2010**, *20*, 1552.
[17] V. Corradini, C. Cervetti, A. Ghirri, R. Biagi, U. del Pennino, G. A. Timco, R. E. P. Winpenny, M. Affronte, *New J. Chem.* **2011**, *35*, 1683.
[18] A. Ghirri, V. Corradini, V. Bellini, R. Biagi, U. del Pennino, V. De Renzi, J. C. Cezar, C. A. Muryn, G. A. Timco, R. E. P. Winpenny, M. Affronte, *ACS Nano.* **2011**, *5*, 7090.
[19] M. Rancan, F. Sedona, M. Di Marino, L. Armelao, M. Sambi, *Chem. Commun.* **2011**, *47*, 5744.
[20] M. Mannini, F. Pineider, C. Danieli, F. Totti, L. Sorace, Ph. Sainctavit, M.-A. Arrio, E. Otero, L. Joly, J. C. Cezar, A. Cornia, R. Sessoli, *Nature* **2010**, *468*, 417.
[21] R. Biagi, J. Fernandez-Rodriguez, M. Gonidec, A. Mirone, V. Corradini, F. Moro, V. De Renzi, U. del Pennino, J. C. Cezar, D. B. Amabilino, J. Veciana, *Phys. Rev. B* **2010**, *82*, 224406.
[22] S. Stepanow, A. Mugarza, G. Ceballos, P. Moras, J. C. Cezar, C. Carbone,, P. Gambardella, *Phys. Rev. B* **2010**, *82*, 014405.
[23] P. Gambardella, S. Stepanow, A. Dmitriev, J. Honolka, F. M. F. de Groot, M. Lingenfelder, S. S. Gupta, D. D. Sarma, P. Bencok, S. Stanescu, S. Clair, S. Pons, N. Lin, A. P. Seitsonen, H. Brune, J. V. Barth, K. Kern, *Nat. Mater.* **2009**, *8*, 189.
[24] S. Stepanow, J. Honolka, P. Gambardella, L. Vitali, N. Abdurakhmanova, T.-C. Tseng, S. Rauschenbach, S.-L. Tait, V. Sessi, S. Klyatskaya, M. Ruben, K. Kern, *J. Am. Chem. Soc.* **2010**, *132*, 11900.
[25] A. Lodi Rizzini, C. Krull, T. Balashov, J. J. Kavich, A. Mugarza, P. S. Miedema, P. K. Thakur, V. Sessi, S. Klyatskaya, M. Ruben, S. Stepanow,, P. Gambardella, *Phys. Rev. Lett.* **2011**, *107*, 177205.
[26] L. Margheriti, D. Chiappe, M. Mannini, P.-E. Car, P. Sainctavit, M.-A. Arrio, F. Buatier de Mongeot, J. C. Cezar, F. M. Piras, A. Magnani, E. Otero, A. Caneschi, R. Sessoli, *Adv. Mater.* **2010**, *22*, 5488.
[27] M. Mannini, E. Tancini, L. Sorace, P. Sainctavit, M.-A. Arrio, Y. Qian, E. Otero, D. Chiappe, L. Margheriti, J. C. Cezar, R. Sessoli, A. Cornia, *Inorg. Chem.* **2011**, *50*, 2911.
[28] S. Carretta, P. Santini, G. Amoretti, T. Guidi, J. R. D. Copley, Y. Qiu, R. Caciuffo, G. Timco,, R. E. P. Winpenny, *Phys. Rev. Lett.* **2007**, *98*, 167401.
[29] V. Corradini, F. Moro, R. Biagi, U. del Pennino, V. De Renzi, S. Carretta, P. Santini, M. Affronte, J. C. Cezar, G. Timco, R. E. P. Winpenny, *Phys. Rev. B* **2008**, *77*, 014402.
[30] C. T. Chen, Y. U. Idzerda, H. J. Lin, N. V. Smith, G. Meigs, E. Chaban, G. H. Ho, E. Pellegrin,, F. Sette, *Phys. Rev. Lett.* **1995**, *75*, 152.
[31] V. Corradini, A. Ghirri, U. del Pennino, R. Biagi, V. A. Milway, G. Timco, F. Tuna, R. E. P. Winpenny, M. Affronte, *Dalton Trans.* **2010**, *39*, 4928.
[32] A. Ghirri, G. Lorusso, F. Moro, V. Corradini, M. Affronte, C. Muryn, F. Tuna, G. Timco, R. E. P. Winpenny, *Phys. Rev. B* **2009**, *79*, 224430.
[33] G. Lorusso, V. Corradini, A. Candini, A. Ghirri, R. Biagi, U. del Pennino, S. Carretta, E. Garlatti, P. Santini, G. Amoretti, G. Timco, R. E. P. Winpenny, M. Affronte, *Phys. Rev. B* **2010**, *82*, 144420.
[34] J. P. Crocombette, B. T. Thole, F. Jollet, *J. Phys.: Condens. Matter* **1996**, *8*, 4095.
[35] F. Troiani, A. Ghirri, M. Affronte, S. Carretta, P. Santini, G. Amoretti, S. Piligkos, G. Timco, R. E. P. Winpenny, *Phys. Rev. Lett.* **2005**, *94*, 207208.
[36] R. Caciuffo, T. Guidi, G. Amoretti, S. Carretta, E. Liviotti, P. Santini, C. Mondelli, G. Timco, C. A. Muryn,, R. E. P. Winpenny, *Phys. Rev. B* **2005**, *71*, 174407.
[37] S. Carretta, P. Santini, G. Amoretti, M. Affronte, A. Ghirri, I. Sheikin, S. Piligkos, G. Timco,, R. E. P. Winpenny, *Phys. Rev. B* **2005**, *72*, 060403.
[38] The axial dipole-dipole interaction and single ion axial anisotropies have similar effects: therefore, d parameters have been rescaled to $d_{Cr} = -0.037$ meV and $d_{Ni} = -0.43$ meV, in order to reproduce the effects of the whole anisotropy.
[39] E. Liviotti, S. Carretta,, G. Amoretti, *Ref. J. Chem. Phys.* **2002**, *117*, 3361.
[40] A. Bencini, D. Gatteschi, *EPR of Exchange Coupled Systems*, Springer Verlag, Berlin-Heidelberg **1990**.
[41] P. Blaha, K. Schwarz, G.K.H. Madsen, D. Kvasnicka, J. Luitz, *WIEN2k, An Augmented Plane Wave +Local Orbitals Program for Calculating Crystal Properties*, Karlheinz Schwarz, Techn. Universität Wien, Austria, **2001**.
[42] D. Tomecka, V. Bellini, F. Troiani, F. Manghi, G. Kamieniarz, M. Affronte, *Phys. Rev. B* **2008**, *77*, 224401.
[43] P. Bruno, *Phys. Rev. B* **1989**, *39*, 865.
[44] F. Troiani, M. Affronte, *Chem. Soc. Rev.* **2011**, *40*, 3119.
[45] S. Carretta, J. van Slageren, T. Guidi, E. Liviotti, C. Mondelli, D. Rovai, A. Cornia, A. L. Dearden, F. Carsughi, M. Affronte, C. D. Frost, R. E. P. Winpenny, D. Gatteschi, G. Amoretti, R. Caciuffo, *Phys. Rev. B* **2003**, *67*, 094405.